

# MixCache: Mixture-of-Cache for Video Diffusion Transformer Acceleration

Yuanxin Wei<sup>1</sup> Lansong Diao<sup>2</sup> Bujiao Chen<sup>2</sup> Shenggan Cheng<sup>3</sup>  
 Zhengping Qian<sup>2</sup> Wenyuan Yu<sup>2</sup> Nong Xiao<sup>1</sup> Wei Lin<sup>2†</sup> Jiangsu Du<sup>1†</sup>

<sup>1</sup>Sun Yat-sen University <sup>2</sup>Alibaba Group <sup>3</sup>National University of Singapore  
 † Corresponding authors

## Abstract

Leveraging the Transformer architecture and the diffusion process, video DiT models have emerged as a dominant approach for high-quality video generation. However, their multi-step iterative denoising process incurs high computational cost and inference latency. Caching, a widely adopted optimization method in DiT models, leverages the redundancy in the diffusion process to skip computations in different granularities (e.g., step, cfg, block). Nevertheless, existing caching methods are limited to single-granularity strategies, struggling to balance generation quality and inference speed in a flexible manner. In this work, we propose MixCache, a training-free caching-based framework for efficient video DiT inference. It first distinguishes the interference and boundary between different caching strategies, and then introduces a context-aware cache triggering strategy to determine when caching should be enabled, along with an adaptive hybrid cache decision strategy for dynamically selecting the optimal caching granularity. Extensive experiments on diverse models demonstrate that, MixCache can significantly accelerate video generation (e.g., 1.94× speedup on Wan 14B, 1.97× speedup on HunyuanVideo) while delivering both superior generation quality and inference efficiency compared to baseline methods.

## 1 Introduction

Diffusion Transformer (DiT) (Peebles and Xie 2023) has revolutionized video generation by integrating the scalability of the Transformer architecture (Vaswani et al. 2017) with the power of the diffusion process (Ho, Jain, and Abbeel 2020; Rombach et al. 2022), enabling unprecedented quality in video generation. Cutting-edge video DiT models emerge including SD3.0 (Esser et al. 2024), Sora (Brooks et al. 2024), CogVideoX (Yang et al. 2024b) and Wan (Wang et al. 2025). These models have facilitated the development of many meaningful applications, such as text-to-video generation (Khachatryan et al. 2023; Wu et al. 2023), video editing (Wang et al. 2023; Jiang et al. 2025) and video continuation (Yang et al. 2024b).

Despite achieving superior fidelity, the inference of video DiT models relies on an iterative denoising process, which demands substantial computation and hinders time-sensitive deployment. Starting from a random Gaussian noise initial-

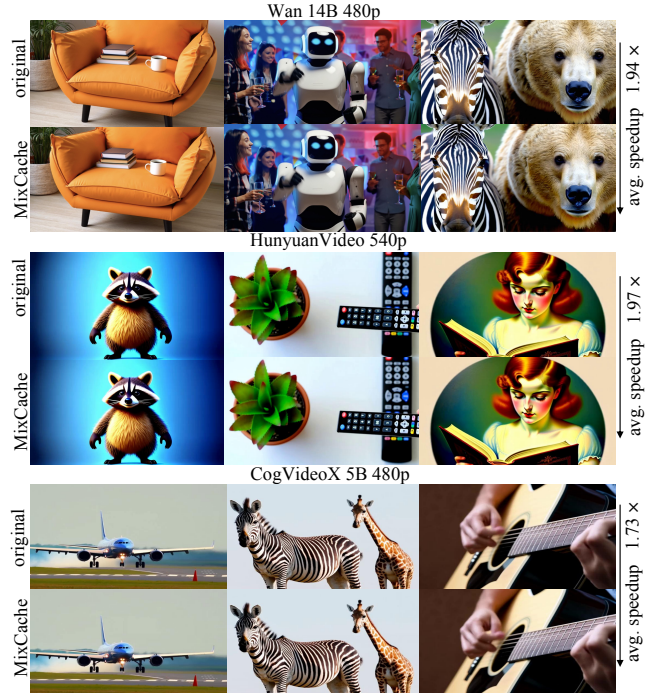


Figure 1: MixCache visualization across video DiT models.

ization, these models require tens of denoising steps, typically ranging from 20 to 100, to progressively reconstruct high-quality video. Consequently, generating a 5-second 720p video with a single GPU can take 50 minutes, presenting a significant latency bottleneck.

The research community has made significant efforts to speed up video DiT models. Among them, caching-based acceleration has emerged as one of the most widely adopted approaches. Caching leverages output similarity across diffusion timesteps by storing and reusing intermediate features, thereby reducing redundant computation and improving efficiency. According to the caching granularity from coarse to fine, existing caching methods can be divided into step level (Liu et al. 2024; Kahatapitiya et al. 2024; Ma et al. 2025), cfg level (Lv et al. 2024), block level (Ma, Fang, and Wang 2024; Wimbauer et al. 2024; Li et al. 2023; Selvaraju

et al. 2024; Zhao et al. 2025; Ma et al. 2024; Shen et al. 2024), and token level (Lou et al. 2024; Zou et al. 2024b,a).

However, existing caching methods primarily exploit output redundancy at a single granularity, overlooking the inherent redundancy across multiple granularities throughout the diffusion process. This narrow focus compromises the balance between generation quality and computational efficiency. Through systematic investigation, we demonstrate that adaptively combining caching methods at diverse granularities enables more effective utilization of output redundancy. In this paper, we propose MixCache, a training-free, caching-based inference framework for video DiT models that enables flexible integration of caching methods with varying granularities. This hybrid caching framework provides more effective acceleration for video DiT inference while preserving generation quality.

Our contributions are as follows:

- We conduct a comprehensive analysis of redundancy across multiple granularities in the diffusion process, including step level, cfg level and block level, and reveal the dynamism nature of redundancy.
- We propose a context-aware cache triggering strategy to determine when to enable caching, along with an adaptive hybrid cache decision strategy to determine the caching granularity (step/cfg/block) in a flexible manner for each timestep.
- Building upon the above strategies, we present MixCache, a training-free caching-based inference framework that adaptively integrates multi-granularity caching methods without modifications to model structure.
- Extensive experiments on industrial-scale video DiT models show that MixCache demonstrates significant improvement in inference speed while maintaining high video quality.

## 2 Related Works

In the following, we introduce important works that are related to our proposed method.

**Step level caching.** Recent DiT advancements introduce diverse step level caching strategies. TeaCache (Liu et al. 2024) leverages input-output correlations by estimating timestep embeddings to implement a dynamic caching. AdaCache (Kahatapitiya et al. 2024) dynamically evaluates step-wise differences to determine skip lengths. AB Cache (Yu et al. 2025) extends prior methods by reusing combined outputs from the previous  $k$  steps, rather than a single-step result. NIRVANA (Agarwal et al. 2024) diverges from these intra-generation approaches by enabling cross-generation cache reuse to skip computation of preceding sampling timesteps.

**CFG level caching.** Recent studies leverage cfg similarities to accelerate diffusion inference. FasterCache (Lv et al. 2024) exploits the similarity between conditional and unconditional outputs at the same timestep to construct a cfg level cache mechanism. DiTFastAttn (Yuan et al. 2024) identifies consistent attention patterns in specific attention heads of conditional and unconditional inference, implementing cfg level attention sharing to bypass redundant computation.

**Block level caching.** For the DiT architecture, recent works propose block level caching with varying strategies. FORA (Selvaraju et al. 2024), PAB (Zhao et al. 2025), and BlockDance (Zhang et al. 2025) employ static interval-based block skipping (e.g., MLP/attention blocks).  $\Delta$ -DiT (Chen et al. 2024) adopts a phase-specific caching strategy, storing back blocks during early stages and front blocks in later stages. L2C (Ma et al. 2024) and MD-DiT (Shen et al. 2024) implement dynamic runtime caching through learnable layer selection and gradient-free search mechanisms, respectively.

**Other optimizations.** Recent works (Lou et al. 2024; Zou et al. 2024b,a; Liu et al. 2025) have explored token redundancy (such as background areas) to reduce computational cost. However, the dynamic nature and dataset-dependent characteristics of input tokens necessitate extensive code modifications to transformer blocks for implementation, resulting in poor compatibility. Moreover, the acceleration efficiency of token level caching is fundamentally limited by its fine-grained caching granularity and the overhead of token importance scoring. In response to the performance bottleneck caused by the multi-step iterative characteristic of the diffusion process, some works also explore efficient solvers, including DDIM (Song, Meng, and Ermon 2021), DPM-Solver (Lu et al. 2022a) and DPM-Solver++ (Lu et al. 2022b). Additionally, distillation-based methods (Salimans and Ho 2022; Luhman and Luhman 2021; Meng et al. 2023) have been developed to compress the number of diffusion sampling timesteps.

## 3 Methodology

### 3.1 Preliminary

**Diffusion model** is a generative model consisting of a forward process and a reverse process. In the forward diffusion process, given an original video  $x_0$  and a random timestep  $t$ , the video after  $t$  diffusion timesteps is:

$$x_t = \sqrt{\delta_t}x_{t-1} + \sqrt{1-\delta_t}\epsilon_t, \quad t = \in [1, T] \quad (1)$$

where  $\delta_t$  is constant related to  $t$ , and  $T$  is the total sampling timesteps. A noise estimation network plays a critical role in approximating the noise distribution in the diffusion process. Specifically, it aims to minimize the discrepancy between the predicted noise term  $\epsilon_\theta$  and the actual noise  $\epsilon$ . In most current works, the noise estimation network adopts the DiT architecture, where the predicted noise function  $\epsilon_\theta(x_t)$  can be further reformulated as:

$$\begin{aligned} \epsilon_\theta(x_t) &= f_{L-1}(f_{L-2}(\dots(f_0(x_t)))) \\ &= f_{L-1} \circ f_{L-2} \circ \dots \circ f_0(x_t) \end{aligned} \quad (2)$$

where  $f_n$  represents the  $n$ -th DiT block and  $L$  represents the total number of DiT blocks.

The inference process, defined as the reverse transformation of noisy data into clean output, is a crucial part of the diffusion process. Initially, a random Gaussian noise  $X_T$  is given. It is input into the noise estimation network  $\epsilon_\theta$  to obtain the noise estimate  $\epsilon_\theta(x_T)$ . According to specific sampling solver  $\Phi$ , the noisy video is denoised to produce the denoised sample  $x_{T-1}$  after one timestep. After iterating this process  $T$  times, the final generated video is obtain.

$$x_{t-1} = \Phi(x_t, t, \epsilon_\theta(x_t)), \quad t = \in [T, 1] \quad (3)$$

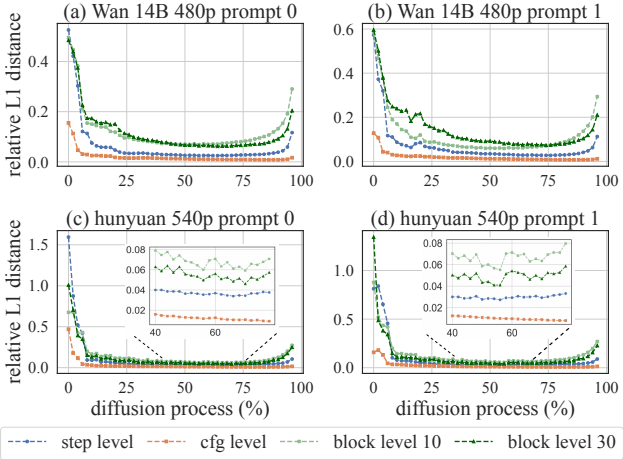


Figure 2: Three levels of redundancy across denoising timesteps in Wan 14B 480p and HunyuanVideo 540p.

**Classifier-Free Guidance (CFG)** has proven to be a powerful technique for improving the fidelity of generated videos in diffusion models. During the sampling process, CFG generates two distinct predictions: the conditional output  $\epsilon_\theta(x_t, t, c)$  conditioned on the input context  $c$ , and the unconditional output  $\epsilon_\theta(x_t, t, \phi)$  derived from the empty/negative prompt  $\phi$ . The final denoised output is obtained by:

$$\tilde{\epsilon}_\theta(x_t, t, c) = (1 + g) \cdot \epsilon_\theta(x_t, t, c) - g \cdot \epsilon_\theta(x_t, t, \phi) \quad (4)$$

where  $g$  is the guidance scale. While CFG significantly enhances visual quality, it also increases computational cost and inference latency due to the additional computation required for unconditional outputs.

### 3.2 Analysis and Motivation

**Three levels of redundancy.** There exists three levels of redundancy in the diffusion process. The first type refers to the **step level** redundancy, which manifests as high similarity between consecutive timestep outputs. The second type is the **cfg level** redundancy, indicating that the outputs of conditional forward and unconditional forward within the same timestep are similar. The third type is **block level** redundancy, which means that the output of some transformer blocks at this timestep is similar to the output of the same block at the previous timestep. We adopt the relative L1 distance to characterize the similarity of two outputs, and the three-level redundancy is measured as follows:

$$\begin{aligned} D_t^{step} &= \frac{\|O_t^{step} - O_{t-1}^{step}\|_1}{\|O_{t-1}^{step}\|_1} \\ D_t^{cfg} &= \frac{\|O_t^{uncond} - O_t^{cond}\|_1}{\|O_t^{cond}\|_1} \\ D_t^{block_i} &= \frac{\|O_t^{block_i} - O_{t-1}^{block_i}\|_1}{\|O_{t-1}^{block_i}\|_1}, i \in [0, L] \end{aligned} \quad (5)$$

where  $t$  denotes the sampling timestep index, advancing incrementally as the diffusion process progresses. The smaller

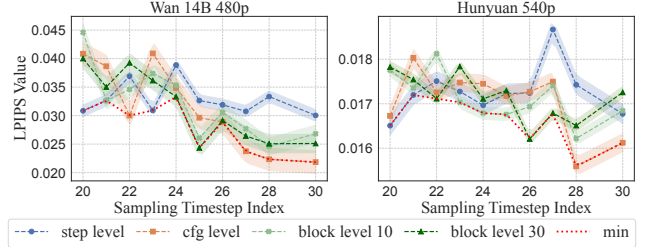


Figure 3: Similarity metric compared with the original model using different cache strategies in different timesteps.

the  $D$  value, the higher the similarity between two outputs. As presented in Figure 2, we use different prompts to examine the different-level redundancy on Wan and Hunyuan-Video. Such redundancy offers opportunities for caching-based computation skipping to enhance inference efficiency.

**The dynamism of redundancy.** In Figure 2, the redundancy during the diffusion process shows strong dynamism. Specifically, there are the following manifestations: (1) All of the three-level redundancy demonstrates strong correlations across timesteps: the initial distance value is relatively high, and gradually decreases and stabilizes. This indicates that the early diffusion stage is sensitive with low redundancy, thereby making it unsuitable for caching. (2) The speed at which redundancy decreases varies among different prompts. (3) The degree of redundancy varies with different levels. For example, in Wan, the cfg level redundancy always remains the strongest throughout the diffusion process. The redundancy of block 10 in the early diffusion stage is stronger than that of block 30, while it is weaker than block 30 in the later diffusion stage. The above phenomena necessitate an adaptive and unified hybrid caching mechanism.

**Potential of three-level cache integration.** We implement different granularity caching methods at each diffusion timestep, and adopt the LPIPS (Zhang et al. 2018) metric to calculate the end-to-end similarity with the original video. The smaller the LPIPS value, the higher the similarity. As shown in Figure 3, the optimal cache granularity varies dynamically across timesteps, suggesting that adaptive cache selection could enhance generation quality.

In order to better integrate different caching granularities, there are two core issues: (1) When will caching be triggered? That is, which timesteps enable caching and which perform full computation? (2) Which caching granularity should be selected for a given cache enabled timestep? To address the above issues, we propose the context-aware cache triggering strategy and adaptive hybrid cache decision strategy, respectively. Integrating these two strategies, we propose the MixCache framework, aiming to achieve video DiT inference acceleration while maintaining a comparable quality of video generation. The overall MixCache framework is demonstrated in Figure 4.

### 3.3 Context-aware Cache Triggering

As the early diffusion stage is responsible for overall framework sketching, it is highly sensitive to interference at this

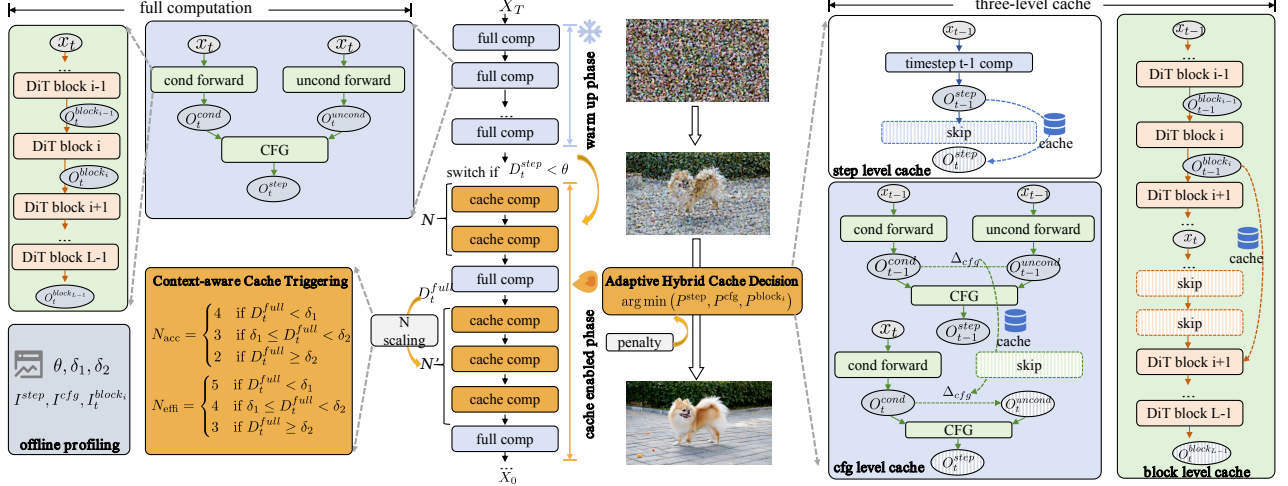


Figure 4: The MixCache framework.

time, as described in SRDiffusion (Cheng et al. 2025). This phenomenon can also be validated in Figure 2, where in the initial diffusion process, the three-level redundancy is relatively low. Therefore, we perform full computation in the initial diffusion stage, and calculate  $D_t^{step}$  between the output of the current timestep  $t$  and that of the previous timestep  $t-1$ , and we call this stage as the *warm up stage*. When  $D_t^{step}$  is smaller than the predefined threshold  $\theta$ , established in the offline profiling process (detailed later), the warm up phase ends and enters the *cache enabled phase*.

Once entering the cache enabled phase, in order to ensure the quality of video generation, it is necessary to perform full computation at certain intervals. A key issue is to determine which timesteps to perform full computation, and we refer to the number of cache enabled steps between two full computation timesteps as *cache interval* (represented as  $N$  in Figure 4). In Figure 2, we observed that, after the warm up phase, the step level redundancy stabilizes at a certain value. Based on this, we propose an adaptive  $N$  scaling strategy designed to dynamically monitor the deviation magnitude between the cached output and the ground-truth output, and automatically adjust the cache interval to maintain generation quality. Specifically, after entering the cache enabled phase, we compare the output of two consecutive full computation, namely  $D^{full}$ , measured in relative L1 distance. When  $D^{full}$  exceeds threshold  $\delta_2$ , this indicates the current cache granularity is too aggressive, requiring a reduction in the subsequent cache interval. Conversely, if it falls below  $\delta_1$ , the next cache interval should be increased. In order to balance quality and efficiency, we provide two cache interval configurations, namely 2/3/4 ( $N_{acc}$ ) and 3/4/5 ( $N_{eff}$ ), which prioritize accuracy and efficiency respectively. The accuracy-prior cache interval  $N_{acc}$  has a higher full computation frequency, resulting in better video generation quality:

$$N_{acc} = \begin{cases} 4 & \text{if } D_t^{full} < \delta_1 \\ 3 & \text{if } \delta_1 \leq D_t^{full} < \delta_2 \\ 2 & \text{if } D_t^{full} \geq \delta_2 \end{cases} \quad (6)$$

### 3.4 Adaptive Hybrid Cache Decision

After identifying cache enabled timesteps, it is crucial to determine the specific caching granularity for a certain timestep within the three-level caching. The limitation of prior works (Liu et al. 2024, 2025; Ma et al. 2025) is their exclusive focus on similarity of different cache methods while neglecting their differential impact on accuracy. To assess the accuracy impact of different caching methods, we generate Gaussian distribution with predefined statistical parameters (mean  $\hat{\mu}$ , standard deviation  $\hat{\sigma}$ ) and calculate the distance between perturbed and original outputs. It should be noted that  $\hat{\mu}$  and  $\hat{\sigma}$  should align with the real parameters derived from the three-level caching. Therefore, we firstly profile prompts and examine the  $\mu$  and  $\sigma$  of the distance tensor between the real output and the cached output. As shown in Figure 6, the  $\mu$  value of the distance tensor is inconsistent across different prompts, and also varies at different timesteps. However, its values are fixed within a certain range. Therefore, we set the  $\hat{\mu}$  value as the average of  $\mu$  value across all timesteps. In addition, for the  $\hat{\sigma}$  value, except for the initial timesteps, it remains stable at a fix value. Therefore, we set the  $\hat{\sigma}$  value as the average of the  $\sigma$  value of the last 40 timesteps. We exclude the first 10 timesteps from analysis since these initial timesteps correspond to the warm up phase without applying caching. Consequently, their outputs lack statistical representativeness for evaluating the proposed methodology.

After determining the  $\hat{\mu}$  and  $\hat{\sigma}$  value, we examine the relative L1 distance between the perturbed output and the original output. We examine for all timesteps and plot the results in Figure 5(a). The smaller the distance, the smaller the impact of the interference on the actual results. This value can indicate the accuracy impact of performing a specific level cache at a specific timestep. From Figure 5(a), it can be seen that the impact value of step level and cfg level remain relatively stable after the warm up phase. However, the block level value exhibits time-dependent characteristics, where its initial value is low, and then increases in the later diffusion

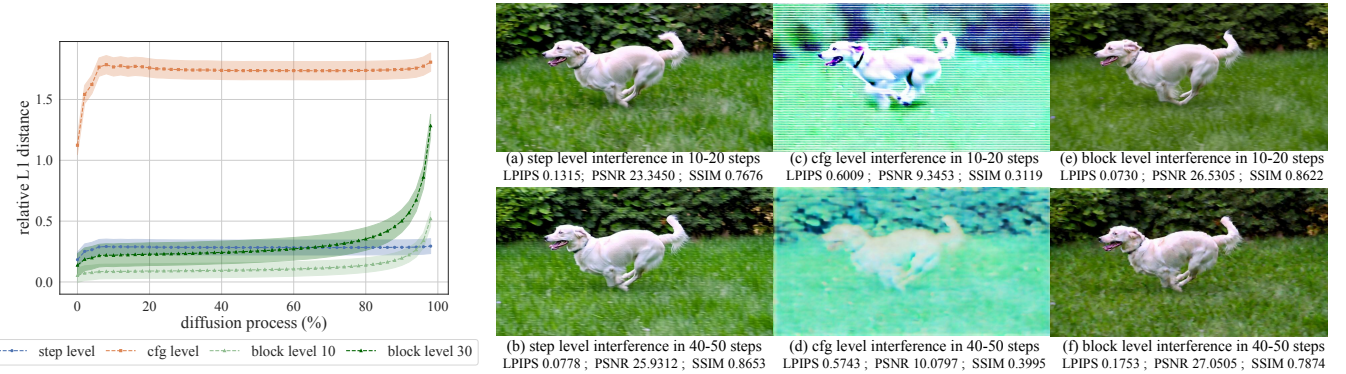


Figure 5: (a) left: Distance between the perturbed and original output, which performs as the impact indicator. (b) right: Visualization and quantitative metrics (LPIPS  $\downarrow$  PSNR  $\uparrow$  SSIM  $\uparrow$ ) of different level interference at different diffusion stages.

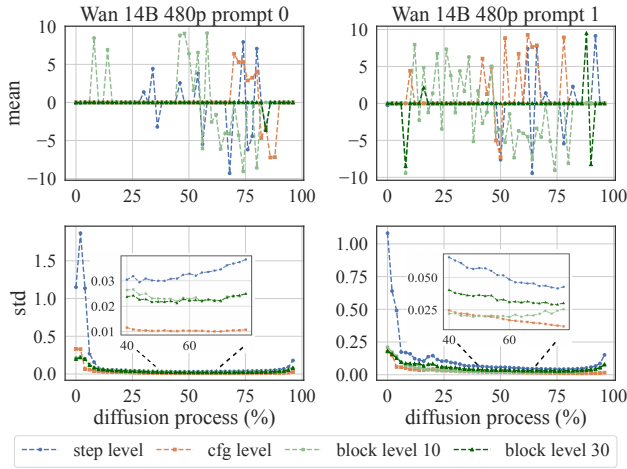


Figure 6: The value of  $\mu$  and  $\sigma$  of the distance tensor between the cached output and the original output.

stage. In addition, the compare across three levels reveals that, the cfg level interference exerts a substantially greater influence, with its value exceeding both step level and block level interference by an order of magnitude. We present the visualized results and similarity metrics in Figure 5(b). It can be seen that the video quality generated using cfg level interference is poor, indicating that this interference has a significant impact on the final results, which is consistent with the conclusion in Figure 5(a). Therefore, the values presented in Figure 5(a) are employed as quantitative evaluation metrics for assessing accuracy impact, with the impact of step level and cfg level remaining constant ( $I_t^{step}$ ,  $I_t^{cfg}$ ), while the block level impact exhibit as a time-dependent and index-dependent function ( $I_t^{block_i}$ ).

The similarity and accuracy impact jointly determine the final generated video quality. We prefer to employ the caching method with a lower similarity and a lower impact, as it indicates that such method exerts minimal influence on the generated video. Therefore, we utilize the product of these two values to represent the final metric, measured as  $P$  value. After each cache enabled timestep, we calculate

the similarity of the three levels and get  $D_t^{step}$ ,  $D_t^{cfg}$ ,  $D_t^{block_i}$ , and product them with the corresponding impact value. Based on the greedy principle, we choose the cache method with the smallest  $P$  as the cache method of the next cache enabled timestep.

$$P_t^\psi = D_t^\psi \cdot I_t^\psi, \psi \in \{step, cfg, block\} \quad (7)$$

In addition, to avoid getting stuck in the same caching granularity within a cache interval, we introduce *penalty* strategy. If a certain cache method is used in this timestep, its  $P$  value in the next timestep will be multiplied by a penalty coefficient, which we set to 5 in our experiments.

### 3.5 Unify it together: MixCache Framework

The context-aware cache triggering strategy and adaptive hybrid cache decision strategy solve the issue of when to enable caching and which cache granularity to select, respectively. Unifying these two strategies, we obtain the MixCache framework. MixCache provides a training-free and adaptive hybrid cache mechanism that can effectively combine three three-level caching, achieving a balance between generation quality and inference speed.

According to Figure 2, the redundancy level of different models varies. Therefore, given a specific model, MixCache will firstly undergo an offline profiling process. During the offline profiling process, MixCache profiles 100 prompts to execute the diffusion process and determines the hyper-parameters  $\theta$ ,  $\delta_1$  and  $\delta_2$ . In addition, the offline profiling also determines the  $\hat{\mu}$  and  $\hat{\sigma}$  of random Gaussian distribution interference, and applies the corresponding interference to determine the impact value of different granularities.

After the offline profiling process, it enters the runtime inference phase. For each prompt, MixCache first applies the context-aware cache triggering strategy to determine which timestep to enable caching. For the cache enabled timesteps, MixCache uses the adaptive hybrid cache decision strategy to determine which of the three-level caching methods to use. The pseudo code of the overall execution process is presented in Appendix A.1.



Figure 7: Visual quality comparison. MixCache delivers high quality and maintains consistency with original results.

## 4 Experiments

### 4.1 Settings

**Base Models and Baselines.** We evaluate MixCache on Wan2.1 14B (Wang et al. 2025), HunyuanVideo (Kong et al. 2024) and CogVideoX 5B (Yang et al. 2024b). For baseline methods, we choose Teacache (Liu et al. 2024), FasterCache (Lv et al. 2024), BlockDance (Zhang et al. 2025) and PAB (Zhao et al. 2025), all of which are specifically designed to accelerate DiT models through caching. Among them, Teacache adopts step level cache, FasterCache combines cfg level and block level cache, and BlockDance and PAB employ block level cache. More implementation details about baseline methods are discussed in Appendix A.2.

**Evaluation Metrics.** To evaluate the quality of video generation, we employ VBench (Huang et al. 2024), a widely-adopted comprehensive benchmarking suite for evaluating video generation. Based on VBench standard prompt set, we use Qwen2.5-14B-Instruct (Yang et al. 2024a) to extend all prompts to enhance the video quality, and generate 5 videos with different seeds for each prompt. In addition, we report LPIPS (Zhang et al. 2018), SSIM (Wang et al. 2004) and PSNR for quality comparison. For efficiency evaluation, we quantify the average inference latency per prompt as the primary performance metric.

**Experiment Settings.** For the main results, we generated 4720 videos for each set of results based on VBench. These were processed in data parallel across a public cloud instance with 64 NVIDIA A800 (80GB) GPUs, and the whole experiment takes nearly a month to complete. In the ablation study, we randomly sample 200 prompts from VBench to conduct experiments, each using 1 seed for generation.

**Implementation Details.** For block level caching, more block candidates will generate larger memory overhead, and even cause OOM error; Fewer block indexes will lose cache flexibility. Therefore, we pre-defined block index as 10, 20, and 30 as candidate block cache objects. More details about the offline profiling are presented in Appendix A.3.

### 4.2 Main Results

**Quantitative Comparison.** Table 1 presents a quantitative comparison of MixCache with baselines in terms of efficiency and visual quality. The results highlight that, MixCache consistently demonstrates robust acceleration efficiency and maintains visually compelling quality across diverse base models, baselines, and resolutions. Full VBench scores are shown in the Appendix.

Methods	Visual Quality				Efficiency	
	Vbench↑	LPIPS↓	PSNR↑	SSIM↑	Latency	Speedup
<b>Wan 14B</b> (832×480, 5s, 81 frames, T = 50)						
<b>original</b>	84.05	-	-	-	900 s	-
Teacache <sub>0.1</sub>	<b>84.01</b>	0.147	22.17	0.786	849 s	1.06 ×
Teacache <sub>0.14</sub>	83.95	0.244	18.60	0.688	612 s	1.47 ×
FasterCache	83.40	0.140	23.26	0.796	633 s	1.42 ×
BlockDance <sub>4</sub>	83.48	0.129	<b>24.01</b>	0.811	679 s	1.29 ×
PAB <sup>8</sup> <sub>100,800</sub>	83.00	0.166	22.29	0.772	717 s	1.25 ×
<b>MixCache<sub>acc</sub></b>	83.97	<b>0.124</b>	23.45	<b>0.814</b>	528 s	1.70 ×
<b>MixCache<sub>effi</sub></b>	83.90	0.132	22.94	0.804	<b>465 s</b>	<b>1.94 ×</b>
<b>Wan 14B</b> (1280×720, 5s, 81 frames, T = 50)						
<b>original</b>	83.66	-	-	-	3168 s	-
Teacache <sub>0.1</sub>	83.75	0.148	22.58	0.813	2988 s	1.06 ×
Teacache <sub>0.14</sub>	<b>83.78</b>	0.237	19.24	0.732	2155 s	1.47 ×
FasterCache	83.12	0.156	22.97	0.806	2230 s	1.42 ×
BlockDance <sub>4</sub>	83.43	0.136	23.70	0.820	2455 s	1.29 ×
PAB <sup>8</sup> <sub>100,800</sub>	83.32	0.195	21.41	0.775	2534 s	1.25 ×
<b>MixCache<sub>acc</sub></b>	83.74	<b>0.132</b>	<b>23.88</b>	<b>0.824</b>	1951 s	1.62 ×
<b>MixCache<sub>effi</sub></b>	83.70	0.146	22.81	0.815	<b>1742 s</b>	<b>1.82 ×</b>
<b>HunyuanVideo</b> (960×544, 5s, 129 frames, T = 50)						
<b>original</b>	81.13	-	-	-	2289 s	-
Teacache <sub>0.1</sub>	80.87	0.247	17.57	0.734	1421 s	1.61 ×
BlockDance <sub>4</sub>	80.93	0.051	<b>28.80</b>	0.897	1646 s	1.39 ×
PAB <sup>8</sup> <sub>100,800</sub>	80.64	0.066	28.56	0.901	1847 s	1.24 ×
<b>MixCache<sub>acc</sub></b>	<b>81.05</b>	<b>0.047</b>	28.37	<b>0.921</b>	1240 s	1.84 ×
<b>MixCache<sub>effi</sub></b>	80.98	0.060	26.86	0.906	<b>1151 s</b>	<b>1.97 ×</b>
<b>CogVideoX 5B</b> (820×480, 6s, 49 frames, T = 50)						
<b>original</b>	80.89	-	-	-	443 s	-
Teacache <sub>0.1</sub>	<b>80.15</b>	0.239	20.42	0.741	289 s	1.53 ×
BlockDance <sub>4</sub>	74.34	0.349	24.76	0.750	348 s	1.27 ×
PAB <sup>8</sup> <sub>100,800</sub>	78.67	0.235	21.69	0.770	293 s	1.51 ×
<b>MixCache<sub>acc</sub></b>	80.10	<b>0.089</b>	<b>34.33</b>	<b>0.892</b>	287 s	1.54 ×
<b>MixCache<sub>effi</sub></b>	<b>80.15</b>	0.160	26.86	0.880	<b>256 s</b>	<b>1.73 ×</b>

Table 1: Comparison of efficiency and visual quality.

**Visual Comparison.** Figure 7 compares the videos generated by MixCache against those by the original model and baselines. The results demonstrate that MixCache can effectively preserve the original semantics and fine details. More visual results are presented in Appendix A.4.

### 4.3 Ablation Study

In the ablation study, we investigate the effects of  $N$  scaling strategy and three-level caching respectively in terms of the visual quality and efficiency. The quantitative results are shown in Table 2 and the corresponding visualization results are presented in Figure 8. Among them, “hybrid” refers to using the adaptive hybrid cache decision strategy to determine the cache method for each timestep, while “step/cfg/block only” refers to using only a specific caching method. “ $N=4$ ” represents a fixed cache interval of 4, and “ $N_{\text{effi}}$ ” represents enabling the  $N$  scaling strategy that prioritizes efficiency. It can be seen that MixCache outperforms all ablation experiments in both quality and efficiency metrics, indicating that combining dynamic  $N$  scaling and three-level caching can achieve better generation quality and inference efficiency. Among them, “cfg only+ $N_{\text{effi}}$ ” can achieve generation quality comparable to MixCache, as the cfg level redundancy is very high (reflected in Figure 1 where its relative L1 distance is small). However, due to its limited computation skip proportion, it is far inferior to MixCache in terms of efficiency.

Method	LPIPS ↓	PSNR ↑	SSIM ↑	Latency	Speedup
original	-	-	-	900 s	-
hybrid + $N=4$	0.082	25.74	0.854	593 s	1.51 ×
step only + $N_{\text{effi}}$	0.147	22.25	0.775	545 s	1.65 ×
cfg only+ $N_{\text{effi}}$	0.080	25.90	0.853	623 s	1.44 ×
block only+ $N_{\text{effi}}$	0.114	24.62	0.809	537 s	1.67 ×
MixCache <sub>effi</sub>	<b>0.079</b>	<b>25.91</b>	<b>0.858</b>	<b>465 s</b>	<b>1.94 ×</b>

Table 2: The ablation study of  $N$  scaling strategy and three-level caching on Wan 14B 480p.

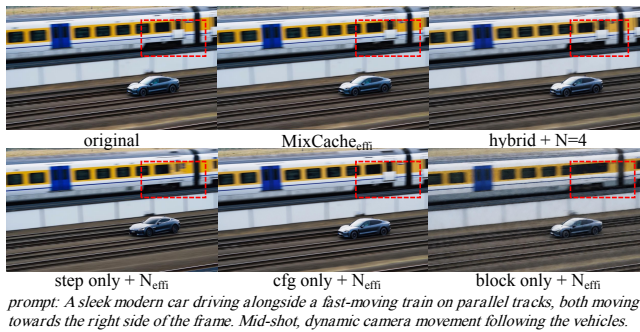


Figure 8: Visualization of ablation study on Wan 14B 480p.

### 4.4 Adaptability

As shown in Figure 9, we present the distribution of three-level caching across three models, evaluated on two distinct prompts. Through intra-model comparison across different prompts, it is evident that both the number of cache enabled timesteps and the distribution across three levels ex-

hibit significant variations. Inter-model analysis reveals distinct cache utilization patterns. For instance, CogVideoX exhibits relatively fewer step level caching compared to other models, which attributes to its unique architectural property. These observations highlight the inherent adaptability of MixCache in accommodating diverse model architectures and prompts through context-aware resource allocation.

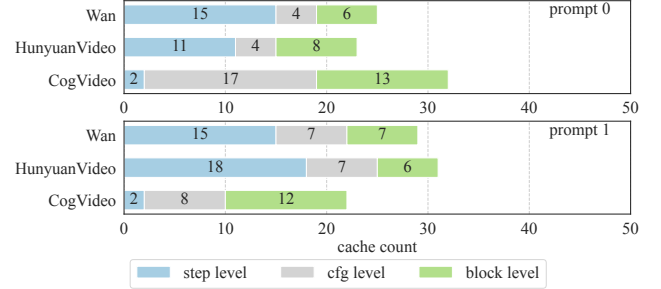


Figure 9: Distribution of three-level caching on two prompts.

### 4.5 Scaling to More GPUs and Higher Resolution

MixCache can be compatible with the current mainstream DiT parallel methods with a minor cache selection synchronization overhead. We integrate Ulysses parallel (Jacobs et al. 2023) to MixCache and present the latency on Wan 14B. As in Figure 10, the parallel version of MixCache still demonstrates a consistent strong scaling with increasing GPU configurations. Besides, this performance advantage is maintained across varying resolutions, demonstrating its effectiveness on high-resolution video generation tasks.

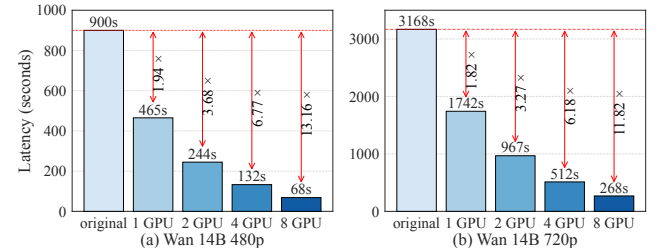


Figure 10: Acceleration efficiency of MixCache with different video resolutions and GPU configurations.

## 5 Conclusion

To address the high-latency challenge of video DiT inference caused by its multi-step iterative denoising process, we propose MixCache, a training-free caching-based framework for efficient video DiT inference. By leveraging the redundancy in the diffusion process of different granularities and adaptively combines three-level caching (step/cfg/block), MixCache achieves comparable generation quality while significantly improving inference efficiency, outperforming existing baselines with a maximum speedup of  $1.94 \times$  on Wan 14B and  $1.97 \times$  on HunyuanVideo. This study establishes hybrid caching as a novel and effective approach for accelerating video DiT inference while maintaining quality.

## References

Agarwal, S.; Mitra, S.; Chakraborty, S.; Karanam, S.; Mukherjee, K.; and Saini, S. K. 2024. Approximate Caching for Efficiently Serving Text-to-Image Diffusion Models. In Vanbever, L.; and Zhang, I., eds., *21st USENIX Symposium on Networked Systems Design and Implementation, NSDI 2024, Santa Clara, CA, April 15-17, 2024*. USENIX Association.

Brooks, T.; Peebles, B.; Holmes, C.; DePue, W.; Guo, Y.; Jing, L.; Schnurr, D.; Taylor, J.; Luhman, T.; Luhman, E.; et al. 2024. Video generation models as world simulators. *OpenAI Blog*, 1: 8.

Chen, P.; Shen, M.; Ye, P.; Cao, J.; Tu, C.; Bouganis, C.; Zhao, Y.; and Chen, T. 2024.  $\Delta$ -DiT: A Training-Free Acceleration Method Tailored for Diffusion Transformers. *CoRR*, abs/2406.01125.

Cheng, S.; Wei, Y.; Diao, L.; Liu, Y.; Chen, B.; Huang, L.; Liu, Y.; Yu, W.; Du, J.; Lin, W.; and You, Y. 2025. SRDiffusion: Accelerate Video Diffusion Inference via Sketching-Rendering Cooperation. *CoRR*, abs/2505.19151.

Esser, P.; Kulal, S.; Blattmann, A.; Entezari, R.; Müller, J.; Saini, H.; Levi, Y.; Lorenz, D.; Sauer, A.; Boesel, F.; Podell, D.; Dockhorn, T.; English, Z.; and Rombach, R. 2024. Scaling Rectified Flow Transformers for High-Resolution Image Synthesis. In *Forty-first International Conference on Machine Learning, ICML 2024, Vienna, Austria, July 21-27, 2024*. OpenReview.net.

Ho, J.; Jain, A.; and Abbeel, P. 2020. Denoising Diffusion Probabilistic Models. In Larochelle, H.; Ranzato, M.; Hadsell, R.; Balcan, M.; and Lin, H., eds., *Advances in Neural Information Processing Systems 33: Annual Conference on Neural Information Processing Systems 2020, NeurIPS 2020, December 6-12, 2020, virtual*.

Huang, Z.; He, Y.; Yu, J.; Zhang, F.; Si, C.; Jiang, Y.; Zhang, Y.; Wu, T.; Jin, Q.; Chanpaisit, N.; et al. 2024. Vbench: Comprehensive benchmark suite for video generative models. In *Proceedings of the IEEE/CVF Conference on Computer Vision and Pattern Recognition*, 21807–21818.

Jacobs, S. A.; Tanaka, M.; Zhang, C.; Zhang, M.; Song, S. L.; Rajbhandari, S.; and He, Y. 2023. DeepSpeed Ulysses: System Optimizations for Enabling Training of Extreme Long Sequence Transformer Models. *CoRR*, abs/2309.14509.

Jiang, Z.; Han, Z.; Mao, C.; Zhang, J.; Pan, Y.; and Liu, Y. 2025. VACE: All-in-One Video Creation and Editing. *CoRR*, abs/2503.07598.

Kahatapitiya, K.; Liu, H.; He, S.; Liu, D.; Jia, M.; Zhang, C.; Ryoo, M. S.; and Xie, T. 2024. Adaptive Caching for Faster Video Generation with Diffusion Transformers. *CoRR*, abs/2411.02397.

Khachatryan, L.; Movsisyan, A.; Tadevosyan, V.; Henschel, R.; Wang, Z.; Navasardyan, S.; and Shi, H. 2023. Text2Video-Zero: Text-to-Image Diffusion Models are Zero-Shot Video Generators. In *IEEE/CVF International Conference on Computer Vision, ICCV 2023, Paris, France, October 1-6, 2023*, 15908–15918. IEEE.

Kong, W.; Tian, Q.; Zhang, Z.; Min, R.; Dai, Z.; Zhou, J.; Xiong, J.; Li, X.; Wu, B.; Zhang, J.; et al. 2024. Hunyuan-video: A systematic framework for large video generative models. *arXiv preprint arXiv:2412.03603*.

Li, S.; Hu, T.; Khan, F. S.; Li, L.; Yang, S.; Wang, Y.; Cheng, M.; and Yang, J. 2023. Faster Diffusion: Rethinking the Role of UNet Encoder in Diffusion Models. *CoRR*, abs/2312.09608.

Liu, D.; Zhang, J.; Li, Y.; Yu, Y.; Lengerich, B.; and Wu, Y. N. 2025. FastCache: Cache What Matters, Skip What Doesn't. In *Proceedings of the IEEE/CVF Conference on Computer Vision and Pattern Recognition (CVPR) Workshops*.

Liu, F.; Zhang, S.; Wang, X.; Wei, Y.; Qiu, H.; Zhao, Y.; Zhang, Y.; Ye, Q.; and Wan, F. 2024. Timestep Embedding Tells: It's Time to Cache for Video Diffusion Model. *CoRR*, abs/2411.19108.

Lou, J.; Luo, W.; Liu, Y.; Li, B.; Ding, X.; Hu, W.; Cao, J.; Li, Y.; and Ma, C. 2024. Token Caching for Diffusion Transformer Acceleration. *CoRR*, abs/2409.18523.

Lu, C.; Zhou, Y.; Bao, F.; Chen, J.; Li, C.; and Zhu, J. 2022a. DPM-Solver: A Fast ODE Solver for Diffusion Probabilistic Model Sampling in Around 10 Steps. In Koyejo, S.; Mohamed, S.; Agarwal, A.; Belgrave, D.; Cho, K.; and Oh, A., eds., *Advances in Neural Information Processing Systems 35: Annual Conference on Neural Information Processing Systems 2022, NeurIPS 2022, New Orleans, LA, USA, November 28 - December 9, 2022*.

Lu, C.; Zhou, Y.; Bao, F.; Chen, J.; Li, C.; and Zhu, J. 2022b. DPM-Solver++: Fast Solver for Guided Sampling of Diffusion Probabilistic Models. *CoRR*, abs/2211.01095.

Luhman, E.; and Luhman, T. 2021. Knowledge Distillation in Iterative Generative Models for Improved Sampling Speed. *CoRR*, abs/2101.02388.

Lv, Z.; Si, C.; Song, J.; Yang, Z.; Qiao, Y.; Liu, Z.; and Wong, K. K. 2024. FasterCache: Training-Free Video Diffusion Model Acceleration with High Quality. *CoRR*, abs/2410.19355.

Ma, X.; Fang, G.; Mi, M. B.; and Wang, X. 2024. Learning-to-Cache: Accelerating Diffusion Transformer via Layer Caching. In Globersons, A.; Mackey, L.; Belgrave, D.; Fan, A.; Paquet, U.; Tomczak, J. M.; and Zhang, C., eds., *Advances in Neural Information Processing Systems 38: Annual Conference on Neural Information Processing Systems 2024, NeurIPS 2024, Vancouver, BC, Canada, December 10 - 15, 2024*.

Ma, X.; Fang, G.; and Wang, X. 2024. DeepCache: Accelerating Diffusion Models for Free. In *IEEE/CVF Conference on Computer Vision and Pattern Recognition, CVPR 2024, Seattle, WA, USA, June 16-22, 2024*, 15762–15772. IEEE.

Ma, Z.; Wei, L.; Wang, F.; Zhang, S.; and Tian, Q. 2025. MagCache: Fast Video Generation with Magnitude-Aware Cache. *arXiv:2506.09045*.

Meng, C.; Rombach, R.; Gao, R.; Kingma, D. P.; Ermon, S.; Ho, J.; and Salimans, T. 2023. On Distillation of Guided Diffusion Models. In *IEEE/CVF Conference on Computer Vi-*

sion and Pattern Recognition, CVPR 2023, Vancouver, BC, Canada, June 17-24, 2023, 14297–14306. IEEE.

Peebles, W.; and Xie, S. 2023. Scalable Diffusion Models with Transformers. In *IEEE/CVF International Conference on Computer Vision, ICCV 2023, Paris, France, October 1-6, 2023*, 4172–4182. IEEE.

Rombach, R.; Blattmann, A.; Lorenz, D.; Esser, P.; and Ommer, B. 2022. High-Resolution Image Synthesis with Latent Diffusion Models. In *IEEE/CVF Conference on Computer Vision and Pattern Recognition, CVPR 2022, New Orleans, LA, USA, June 18-24, 2022*, 10674–10685. IEEE.

Salimans, T.; and Ho, J. 2022. Progressive Distillation for Fast Sampling of Diffusion Models. In *The Tenth International Conference on Learning Representations, ICLR 2022, Virtual Event, April 25-29, 2022*. OpenReview.net.

Selvaraju, P.; Ding, T.; Chen, T.; Zharkov, I.; and Liang, L. 2024. FORA: Fast-Forward Caching in Diffusion Transformer Acceleration. *CoRR*, abs/2407.01425.

Shen, M.; Chen, P.; Ye, P.; Xia, G.; Chen, T.; Bouganis, C.-S.; and Zhao, Y. 2024. MD-DiT: Step-aware Mixture-of-Depths for Efficient Diffusion Transformers. In *Adaptive Foundation Models: Evolving AI for Personalized and Efficient Learning*.

Song, J.; Meng, C.; and Ermon, S. 2021. Denoising Diffusion Implicit Models. In *9th International Conference on Learning Representations, ICLR 2021, Virtual Event, Austria, May 3-7, 2021*. OpenReview.net.

Vaswani, A.; Shazeer, N.; Parmar, N.; Uszkoreit, J.; Jones, L.; Gomez, A. N.; Kaiser, L.; and Polosukhin, I. 2017. Attention is All you Need. In Guyon, I.; von Luxburg, U.; Bengio, S.; Wallach, H. M.; Fergus, R.; Vishwanathan, S. V. N.; and Garnett, R., eds., *Advances in Neural Information Processing Systems 30: Annual Conference on Neural Information Processing Systems 2017, December 4-9, 2017, Long Beach, CA, USA*, 5998–6008.

Wang, A.; Ai, B.; Wen, B.; Mao, C.; Xie, C.-W.; Chen, D.; Yu, F.; Zhao, H.; Yang, J.; Zeng, J.; et al. 2025. Wan: Open and Advanced Large-Scale Video Generative Models. *arXiv preprint arXiv:2503.20314*.

Wang, X.; Yuan, H.; Zhang, S.; Chen, D.; Wang, J.; Zhang, Y.; Shen, Y.; Zhao, D.; and Zhou, J. 2023. VideoComposer: Compositional Video Synthesis with Motion Controllability. In Oh, A.; Naumann, T.; Globerson, A.; Saenko, K.; Hardt, M.; and Levine, S., eds., *Advances in Neural Information Processing Systems 36: Annual Conference on Neural Information Processing Systems 2023, NeurIPS 2023, New Orleans, LA, USA, December 10 - 16, 2023*.

Wang, Z.; Bovik, A. C.; Sheikh, H. R.; and Simoncelli, E. P. 2004. Image quality assessment: from error visibility to structural similarity. *IEEE transactions on image processing*, 13(4): 600–612.

Wimbauer, F.; Wu, B.; Schönfeld, E.; Dai, X.; Hou, J.; He, Z.; Sanakoyeu, A.; Zhang, P.; and Sam S. Tsai, e. 2024. Cache Me if You Can: Accelerating Diffusion Models through Block Caching. In *IEEE/CVF Conference on Computer Vision and Pattern Recognition, CVPR 2024, Seattle, WA, USA, June 16-22, 2024*, 6211–6220. IEEE.

Wu, J. Z.; Ge, Y.; Wang, X.; Lei, S. W.; Gu, Y.; Shi, Y.; Hsu, W.; Shan, Y.; Qie, X.; and Shou, M. Z. 2023. Tune-A-Video: One-Shot Tuning of Image Diffusion Models for Text-to-Video Generation. In *IEEE/CVF International Conference on Computer Vision, ICCV 2023, Paris, France, October 1-6, 2023*, 7589–7599. IEEE.

Yang, A.; Yang, B.; Hui, B.; Zheng, B.; Yu, B.; Zhou, C.; Li, C.; Li, C.; Liu, D.; Huang, F.; Dong, G.; Wei, H.; Lin, H.; and Jialong Tang, e. 2024a. Qwen2 Technical Report. *arXiv preprint arXiv:2407.10671*.

Yang, Z.; Teng, J.; Zheng, W.; Ding, M.; Huang, S.; Xu, J.; Yang, Y.; Hong, W.; Zhang, X.; Feng, G.; et al. 2024b. Cogvideox: Text-to-video diffusion models with an expert transformer. *arXiv preprint arXiv:2408.06072*.

Yu, Z.; Zou, Z.; Shao, G.; Zhang, C.; Xu, S.; Huang, J.; Zhao, F.; Cun, X.; and Zhang, W. 2025. AB-Cache: Training-Free Acceleration of Diffusion Models via Adams-Bashforth Cached Feature Reuse. *CoRR*, abs/2504.10540.

Yuan, Z.; Zhang, H.; Pu, L.; Ning, X.; Zhang, L.; Zhao, T.; Yan, S.; Dai, G.; and Wang, Y. 2024. DiTFastAttn: Attention Compression for Diffusion Transformer Models. In *Advances in Neural Information Processing Systems 38: Annual Conference on Neural Information Processing Systems 2024, NeurIPS 2024, Vancouver, BC, Canada, December 10 - 15, 2024*.

Zhang, H.; Gao, T.; Shao, J.; and Wu, Z. 2025. BlockDance: Reuse Structurally Similar Spatio-Temporal Features to Accelerate Diffusion Transformers. *CoRR*, abs/2503.15927.

Zhang, R.; Isola, P.; Efros, A. A.; Shechtman, E.; and Wang, O. 2018. The unreasonable effectiveness of deep features as a perceptual metric. In *Proceedings of the IEEE conference on computer vision and pattern recognition*, 586–595.

Zhao, X.; Jin, X.; Wang, K.; and You, Y. 2025. Real-Time Video Generation with Pyramid Attention Broadcast. In *The Thirteenth International Conference on Learning Representations, ICLR 2025, Singapore, April 24-28, 2025*. OpenReview.net.

Zou, C.; Liu, X.; Liu, T.; Huang, S.; and Zhang, L. 2024a. Accelerating Diffusion Transformers with Token-wise Feature Caching. *CoRR*, abs/2410.05317.

Zou, C.; Zhang, E.; Guo, R.; Xu, H.; He, C.; Hu, X.; and Zhang, L. 2024b. Accelerating Diffusion Transformers with Dual Feature Caching. *arXiv preprint arXiv:2412.18911*.

## A Appendix

### A.1 Pseudo code of the MixCache framework

The execution flow of MixCache is formalized in Algorithm 1. The methodology commences with an offline profiling phase to determine the hyper-parameters (line 1). During runtime, one generation is partitioned into two distinct phases: the warm up phase and the cache enabled phase. In the warm up phase, the system exclusively executes full computations to maintain video quality. The cache enabled phase implements a dynamic switching mechanism that alternates between cached computation at three granularities and full computation, utilizing a predefined  $D_t^{\text{step}}$  as the transition criterion (line 5). Once in the cache enabled phase, two core control mechanisms are activated: (1) the  $N$  scaling strategy to regulate the frequency of cache interval, and (2) the adaptive hybrid cache decision strategy (line 23-24) that dynamically determines the optimal caching granularity for each timestep.

Algorithm 1: Pseudo code of the MixCache framework

```

1: Offline Profiling: Obtain  $\theta, \delta_1, \delta_2, I_t^{\text{step}}, I_t^{\text{cfg}}, I_t^{\text{block}_i}$ 
2: Initialize: cache interval  $N, \text{cnt} = 0$ 
3: for each sampling timestep  $t \in \{0, 1, 2, \dots, T - 1\}$  do
4:   Compute  $D_t^{\text{step}}, D_t^{\text{cfg}}, D_t^{\text{block}_i}$ 
5:   if  $D_t^{\text{step}} \geq \theta$  then            $\triangleright$  Warm-up phase
6:     Perform full computation
7:   else                          $\triangleright$  Cache enabled phase
8:      $\text{cnt} \leftarrow (\text{cnt} + 1) \% N$ 
9:     if  $\text{cnt} == 0$  then
10:       Perform full computation
11:       Compute  $D_t^{\text{full}}$  and scale  $N$ 
12:     else if cache mode is step level then
13:        $O_t \leftarrow O_{t-1}$ 
14:     else if cache mode is cfg level then
15:        $O_t^{\text{cond}} \leftarrow$  conditional forward output
16:        $O_t^{\text{uncond}} \leftarrow O_t^{\text{cond}} + \Delta_{\text{cfg}}$ 
17:        $O_t \leftarrow \text{CFG}(O_t^{\text{cond}}, O_t^{\text{uncond}})$ 
18:     else if cache mode is block level  $i$  then
19:       Input for block  $i + 1 \leftarrow O_{t-1}^{\text{block}_i}$ 
20:       Execute DiT block[i+1:]
21:        $O_t^{\text{uncond}} \leftarrow O_t^{\text{cond}} + \Delta_{\text{cfg}}$ 
22:        $O_t \leftarrow \text{CFG}(O_t^{\text{cond}}, O_t^{\text{uncond}})$ 
23:      $P_t^\psi \leftarrow D_t^\psi \cdot I_t^\psi, \psi \in \{\text{step}, \text{cfg}, \text{block}\}$ 
24:     cache mode  $\leftarrow \arg \min(P_t^{\text{step}}, P_t^{\text{cfg}}, P_t^{\text{block}_i})$ 

```

### A.2 Further details of baseline methods

For TeaCache, we use the open-source implementation and adjust the `L1_distance_thresh` parameter to balance quality and speed. Teacache<sub>0.1</sub> indicates that the value of `L1_distance_thresh` is set to 0.1. Increasing the `L1_distance_thresh` enhances acceleration efficiency. However, this improvement comes at the cost of reduced generation quality.

For BlockDance, following the official setting, we set the cache block index as 20 and set the first 40% of denois-

ing steps as warm up steps that disable caching, and evenly divide the remaining 60% of denoising steps into several groups, each comprising  $N$  steps. BlockDance<sub>4</sub> denotes that the  $N$  value equals to 4.

As for PAB, we adopt the implementation from HuggingFace Diffusers, tuning both `block_skip_range` and `timestep_skip_range` to manage the quality-speed trade-off. PAB<sub>100,800</sub><sup>8</sup> denotes a configuration where the `block_skip_range` is set to 8 and the `timestep_skip_range` is set to [100, 800].

### A.3 Further details of the offline profiling process

In the offline profiling phase, we execute 100 prompts to inference to collect operational data for determining runtime hyper-parameters  $(\theta, \delta_1, \delta_2)$ . As this process occurs offline, it requires only a single execution, enabling deployment of these hyper-parameters during runtime without introducing additional computational overhead. As a result, the profiled hyper-parameters  $\theta, \delta_1$  and  $\delta_2$  for Wan and HunyuanVideo are 0.1, 0.05, 0.1, respectively, and those for CogVideoX are 0.1, 0.3, 0.4 respectively.

### A.4 More visualization results

To comprehensively verify the method we proposed, we present additional visual presentation for each DiT model from extended VBench prompts, as indicated in Figure 11 and Figure 12. Our method maintains high-quality with a high degree of consistency and fine details with the video generated by the original models, while achieving significant acceleration.

In addition, we demonstrate the generated videos of three models using the same prompts under different MixCache configurations, including accuracy-prior and efficiency-prior configurations. As shown in Figure 13, these two configurations of MixCache show a highly consistent generation quality with the original video across different prompts and base models, reflecting its effectiveness.

### A.5 Full VBench score for each dimension

Tables 3 and Tables 4 present the detailed VBench scores of Wan, HunyuanVideo and CogVideoX across various dimensions. MixCache can maintain a high VBench score, including the total score and the scores of all dimensions, indicating its advantages over baselines in terms of generation quality.

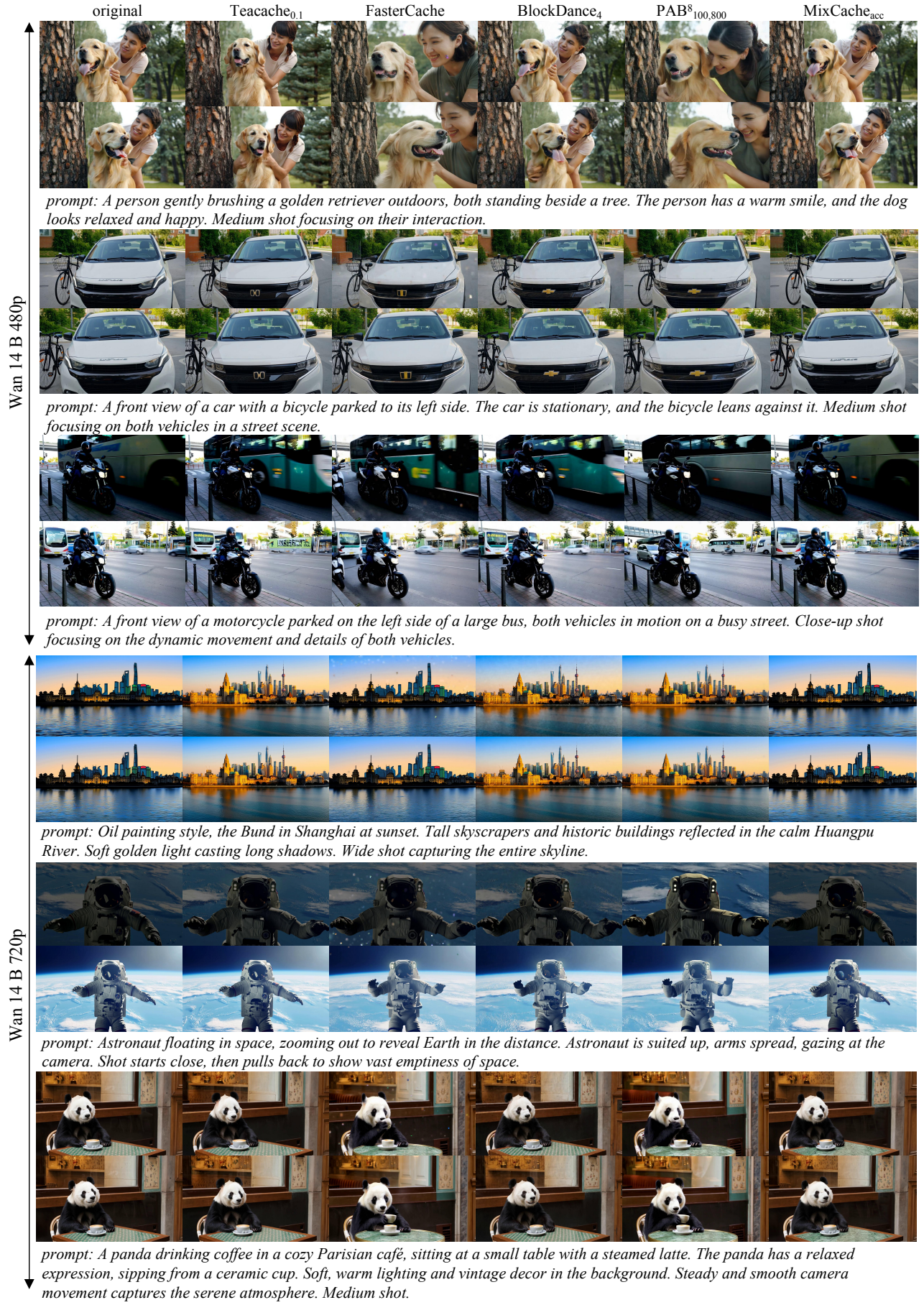


Figure 11: More visualization results of Wan 14B 480p and 720p on extended VBench prompts.

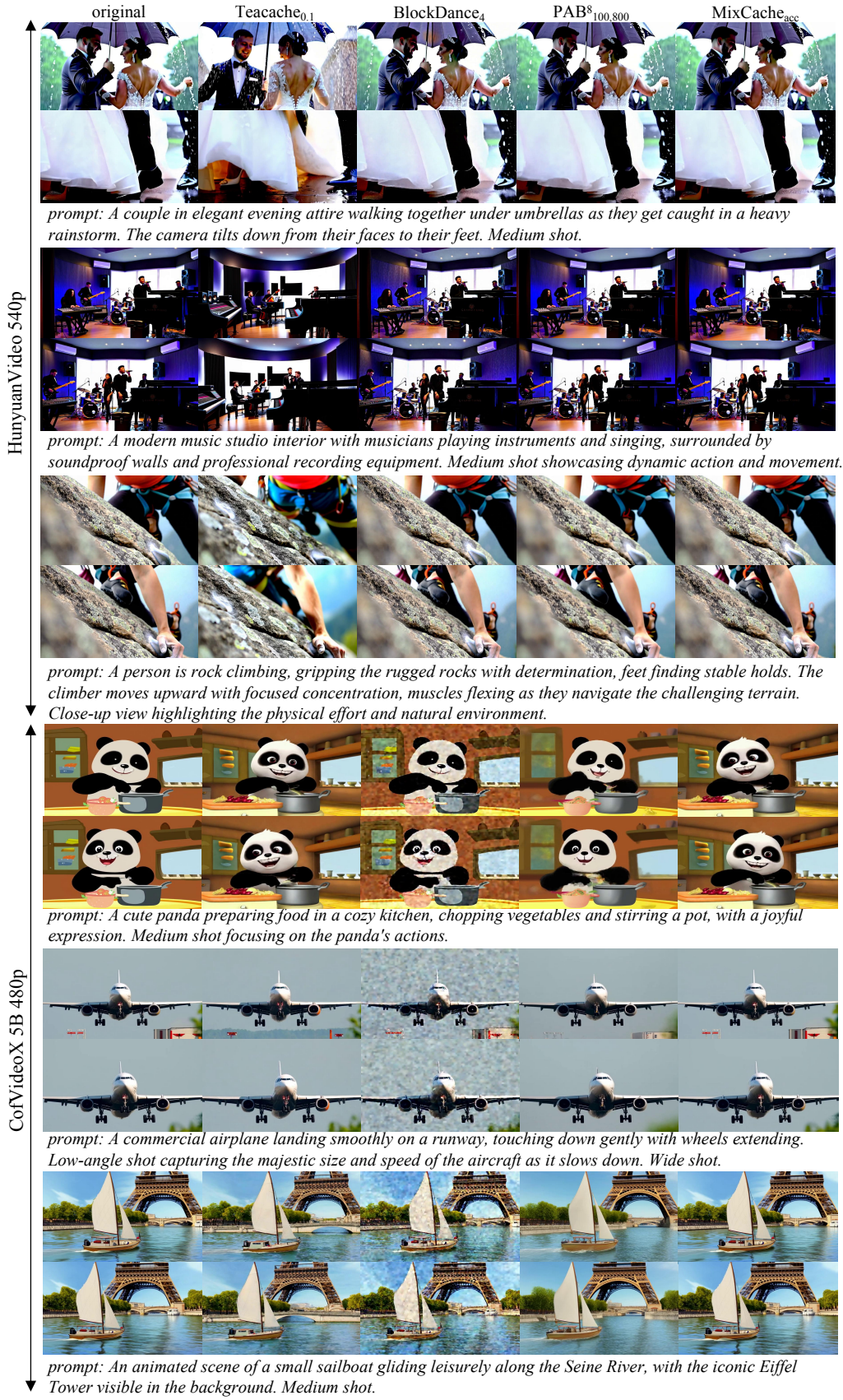
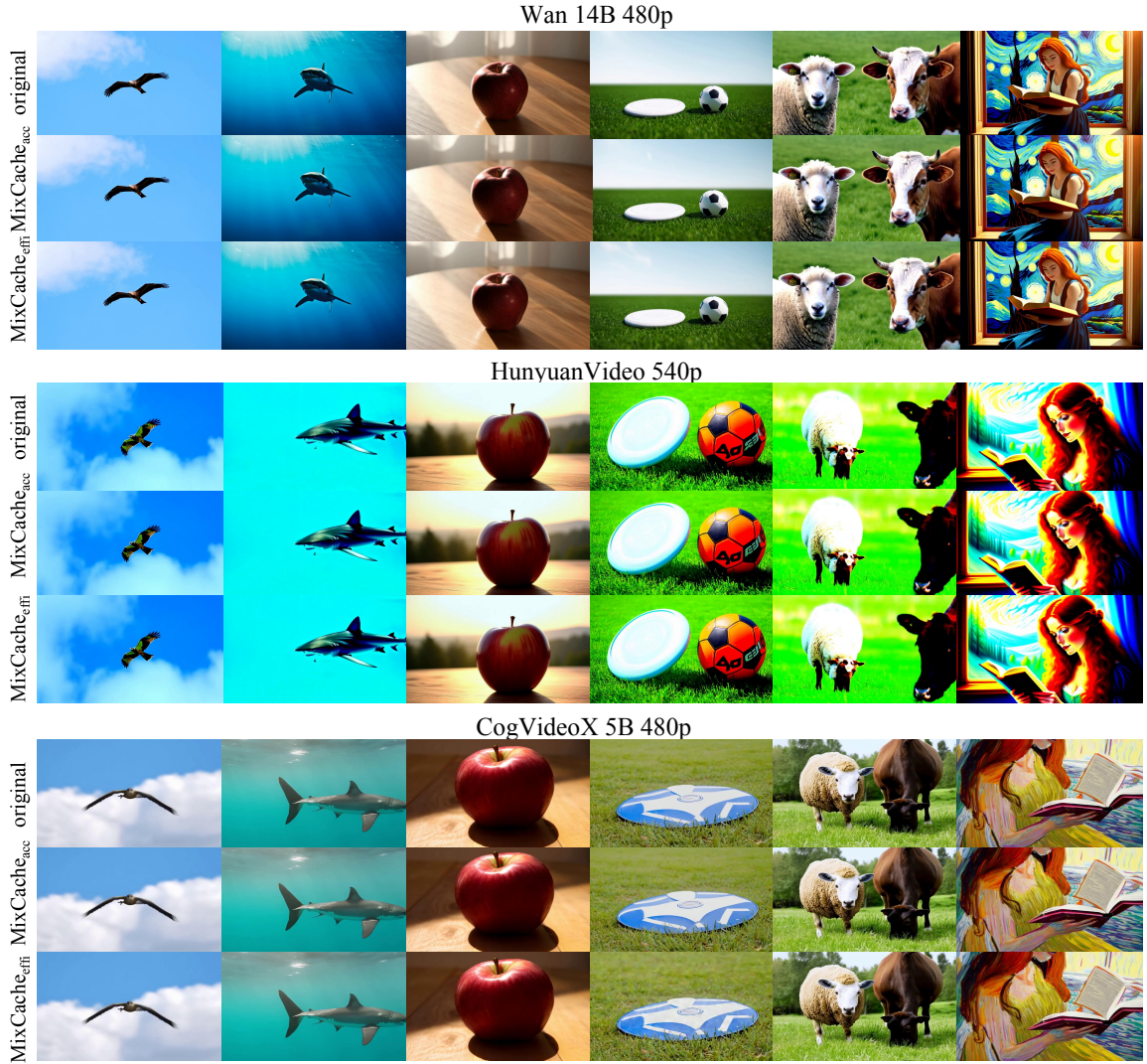


Figure 12: More visualization results of HunyuanVideo 540p and CogVideoX 480p on extended VBench prompts.



*prompt:*

- A realistic flying bird with spread wings, soaring against a bright blue sky filled with soft clouds. Close-up aerial shot focusing on the bird's detailed feathers and movement.
- A large great white shark is swimming gracefully through the vast ocean, with the camera panning right to follow its powerful movements. Medium shot.
- A serene scene of a single ripe red apple resting on a wooden table, surrounded by soft morning light casting gentle shadows. Close-up shot focusing on the texture and shine of the apple.
- A front view of a frisbee on the left and a sports ball on the right, both lying on a grass field. Close-up shot.
- A front view of a sheep on the left and a cow on the right, both grazing in a lush green field. Close-up shot focusing on their faces and expressions.
- Gwen Stacy reading a book in a Van Gogh style painting. She has long red hair and wears a vintage dress, sitting by a window with sunlight casting a warm glow. The background features swirling patterns and vibrant colors typical of Van Gogh's artwork. Close-up view focusing on Gwen's engaged expression as she reads.

Figure 13: Visualization results of accuracy-prior and efficiency-prior configuration on MixCache.

Score	original	Teocache <sub>0.1</sub>	Teocache <sub>0.14</sub>	Fastercache	BlockDance <sub>4</sub>	PAB <sup>8</sup> <sub>100,800</sub>	MixCache <sub>acc</sub>	MixCache <sub>effi</sub>
<b>Wan 14B 480p</b>								
<b>total score</b>	84.05	84.01	83.95	83.40	83.48	83.00	83.97	83.90
quality score	85.04	84.96	84.85	84.26	84.29	83.77	84.89	84.84
semantic score	80.09	80.24	80.34	79.94	80.25	79.95	80.27	80.16
subject consistency	93.91	93.85	93.84	92.87	93.31	93.58	93.97	93.94
background consistency	97.06	97.08	97.08	95.11	95.87	94.46	97.10	97.17
temporal flickering	96.84	96.87	96.82	96.65	96.52	97.11	96.82	96.79
motion smoothness	93.76	93.72	93.86	94.24	93.76	94.37	93.89	93.89
dynamic degree	37.50	37.22	36.95	36.80	36.25	35.41	36.80	36.66
aesthetic quality	66.90	66.77	66.75	65.78	65.84	62.93	66.82	66.77
imaging quality	66.76	66.71	66.22	66.24	66.34	66.62	66.37	66.21
object class	93.09	93.47	93.01	92.29	93.64	92.55	93.20	93.02
multiple objects	81.16	79.10	80.79	81.14	80.66	80.75	81.10	80.66
human action	98.00	97.60	97.40	97.80	98.00	97.80	97.80	97.60
color	84.60	85.08	83.63	83.79	83.83	83.98	84.72	84.94
spatial relationship	78.65	80.53	80.32	79.84	81.22	77.41	79.06	79.08
scene	66.58	67.92	69.81	67.20	66.69	69.20	68.30	68.07
appearance style	77.20	77.02	76.81	76.56	76.88	76.77	76.91	76.88
temporal style	68.35	68.30	68.21	67.77	68.30	68.19	68.30	68.10
overall consistency	73.16	73.13	73.05	73.02	73.08	72.88	73.08	73.10
<b>Wan 14B 720p</b>								
<b>total score</b>	83.66	83.75	83.78	83.12	83.43	83.32	83.74	83.70
quality score	84.66	84.74	84.71	84.08	84.35	84.13	84.76	84.67
semantic score	79.69	79.78	80.05	79.30	79.77	80.06	79.68	79.83
subject consistency	92.45	92.34	92.41	91.39	91.95	92.21	92.34	92.47
background consistency	96.64	96.63	96.59	94.95	95.68	95.13	96.72	96.70
temporal flickering	97.17	97.14	97.11	97.01	96.84	97.41	97.14	97.14
motion smoothness	92.66	92.80	93.00	93.52	93.07	93.45	93.07	93.17
dynamic degree	37.22	38.05	38.05	37.09	37.64	36.80	37.91	37.36
aesthetic quality	65.67	65.58	65.48	64.75	65.01	63.50	65.76	65.63
imaging quality	68.46	68.26	67.99	67.82	68.06	68.34	68.00	67.90
object class	92.01	91.71	91.65	90.76	91.61	91.52	92.14	92.36
multiple objects	78.19	78.93	78.26	76.89	79.13	77.94	78.99	78.75
human action	98.20	98.20	98.00	97.80	98.20	98.20	98.00	97.80
color	86.20	86.69	88.57	85.79	87.59	86.14	86.58	85.36
spatial relationship	76.09	75.93	76.32	75.85	75.68	78.82	75.01	76.58
scene	68.60	69.03	70.04	69.82	68.27	71.31	68.73	70.02
appearance style	76.07	75.72	75.79	75.26	75.65	75.23	75.79	75.72
temporal style	67.77	67.97	67.66	67.53	67.86	67.72	67.86	67.86
overall consistency	74.12	73.85	74.18	73.96	73.98	73.65	73.98	74.01

Table 3: VBench score for all dimensions: Wan 14B 480p and Wan 14B 720p.

Score	original	Teacache <sub>0.1</sub>	BlockDance <sub>4</sub>	PAB <sup>8</sup> <sub>100,800</sub>	MixCache <sub>acc</sub>	MixCache <sub>eff</sub>
<b>HunyuanVideo 540p</b>						
<b>total score</b>	81.13	80.87	80.93	80.64	81.05	80.98
quality score	82.66	82.32	82.28	82.21	82.56	82.51
semantic score	75.04	75.05	75.52	74.36	75.00	74.85
subject consistency	92.86	92.75	92.63	92.77	92.90	92.91
background consistency	95.37	95.36	94.75	95.11	95.46	95.42
temporal flickering	98.22	98.25	97.65	98.11	98.22	98.25
motion smoothness	96.47	96.36	96.12	96.47	96.54	96.60
dynamic degree	31.25	30.28	30.28	30.14	30.84	30.70
aesthetic quality	61.41	61.46	60.96	60.63	61.41	61.41
imaging quality	61.71	60.65	62.41	61.11	61.26	61.05
object class	86.11	87.50	85.97	85.55	86.12	86.31
multiple objects	68.16	67.41	68.43	67.03	66.94	66.28
human action	97.20	97.20	97.20	97.20	97.20	97.60
color	85.09	85.81	86.13	86.56	86.71	85.69
spatial relationship	61.29	61.15	66.04	59.57	61.45	61.69
scene	60.44	59.72	58.74	57.82	59.83	59.64
appearance style	77.72	77.72	77.86	77.51	77.48	77.37
temporal style	66.46	66.87	66.37	65.71	66.48	66.43
overall consistency	72.86	72.09	72.94	72.28	72.77	72.66
<b>CogVideoX 5B 480p</b>						
<b>total score</b>	80.89	80.15	74.34	78.67	80.10	80.15
quality score	82.20	81.22	76.12	80.35	81.42	81.44
semantic score	75.61	75.87	67.24	71.95	74.80	74.99
subject consistency	92.55	91.92	89.20	91.75	92.00	92.04
background consistency	94.48	94.07	93.45	94.08	94.27	94.16
temporal flickering	93.90	93.66	91.96	95.28	93.82	93.80
motion smoothness	92.80	91.90	88.71	93.83	92.18	92.04
dynamic degree	38.47	35.84	15.14	33.75	36.25	36.53
aesthetic quality	60.69	59.95	56.00	58.37	60.02	59.99
imaging quality	61.44	60.60	60.31	55.24	60.71	60.80
object class	87.41	86.16	74.37	81.63	86.11	86.28
multiple objects	65.09	66.01	44.41	56.25	64.27	64.77
human action	98.20	97.80	96.40	96.80	98.00	98.20
color	86.84	87.16	76.28	88.84	87.30	87.66
spatial relationship	55.03	57.60	49.66	48.21	54.31	54.23
scene	66.46	65.60	50.84	59.38	62.79	63.16
appearance style	81.13	81.66	81.62	80.18	81.17	81.10
temporal style	66.87	66.62	61.59	64.31	65.82	65.99
overall consistency	73.46	74.18	70.00	71.92	73.46	73.52

Table 4: VBench score for all dimensions: HunyuanVideo 540p and CogVideoX 5B 480p.